

---

# PROTEIN STRUCTURE PREDICTION IN THE 3D HP MODEL USING DEEP REINFORCEMENT LEARNING

---

**Giovanny Espitia\***  
Department of Physics  
The University of Texas at Austin  
Austin, TX 78712

**Yui Tik Pang**  
School of Physics  
Georgia Institute of Technology  
Atlanta, GA 30332

**James C. Gumbart**  
School of Physics  
Georgia Institute of Technology  
Atlanta, GA 30332

December 31, 2024

## ABSTRACT

We address protein structure prediction in the 3D Hydrophobic-Polar lattice model through two novel deep learning architectures. For proteins under 36 residues, our hybrid reservoir-based model combines fixed random projections with trainable deep layers, achieving optimal conformations with 25% fewer training episodes. For longer sequences, we employ a long short-term memory network with multi-headed attention, matching best-known energy values. Both architectures leverage a stabilized Deep Q-Learning framework with experience replay and target networks, demonstrating consistent achievement of optimal conformations while significantly improving training efficiency compared to existing methods.

## 1 Introduction and Related Work

Simulating protein folding is a fundamental challenge in biophysics and computational biology, yet it is crucial for understanding protein structure, function, and dynamics, with significant implications for drug discovery and disease diagnosis. The Hydrophobic-Polar (HP) model serves as a simplified yet powerful framework for studying protein folding, classifying amino acids as either hydrophobic (H) or polar (P) on a lattice structure. Despite its apparent simplicity, finding optimal conformations in the HP model remains NP-complete, making it particularly challenging for larger proteins. Early approaches to this problem employed various computational methods, including genetic algorithms [Unger and Moult, 1993], Monte Carlo simulations with evolutionary algorithms [Patton et al., 1995], and memetic algorithms with self-adaptive local search [Krasnogor, 2010]. Additional methodologies encompassed ant colony optimization [Shmygelska and Hoos, 2005], core-directed chain growth [Beutler and Dill, 1996], and the pruned-enriched Rosenbluth method (PERM) [Grassberger, 1997]. Recent advances in deep reinforcement learning (DRL) have opened new avenues for addressing the protein folding challenge. Notable contributions include Q-learning approaches [Czibula et al., 2011], hybrid methods combining Q-learning with ant colony optimization [Doğan and Ölmez, 2015], and FoldingZero [Li et al., 2018], which integrates Monte Carlo tree search with convolutional neural networks. Building upon these foundations, we propose two novel architectures: (1) a reservoir computing-based hybrid architecture [Jaeger, 2007] that captures temporal dependencies in the protein folding process and (2) an LSTM network enhanced with multi-head attention layers that effectively models long-range interactions between amino acids [Bahdanau et al., 2015]. These architectural approaches have individually demonstrated success in various domains, including time series prediction [Subramoney et al., 2021], speech recognition [Araujo et al., 2020], and robot control [Antonelo and Schrauwen, 2015]. Our work represents the first application of reservoir computing to the protein folding problem in the 3D HP model, while also introducing an attention-enhanced LSTM architecture specifically designed for longer protein sequences. The reservoir-based approach leverages the computational efficiency of fixed, randomly initialized recurrent neural networks to project input data into high-dimensional space, while the attention mechanism in the LSTM architecture enables effective modeling of interactions between distant amino acids. Both architectures consistently achieve optimal conformations matching the best known energy values while demonstrating improved training efficiency compared to traditional approaches. The remainder of this paper is organized as follows: Section 2

\*Correspondence to gespitia3@utexas.edu  
Preprint. Under review.

formulates the protein folding problem in the 3D HP model as a deep reinforcement learning problem and describes our proposed architectures and training methodology, Section 3 presents experimental results comparing our approach with other state-of-the-art methods and analyzing the role of both the reservoir and attention mechanisms, and Sections 4 and 5 discuss implications and conclude the paper.

## 2 Methodology

In this section, we describe the methods used to model the problem as Markov Decision Process (MDP) and introduce the details of the architectures.

### 2.1 Modeling the problem in a cubic lattice

Let  $\mathcal{G}$  be a 3D cubic lattice with lattice points  $(x, y, z) \in \mathbb{Z}^3$ . Similar to [Yang et al., 2023], the protein folding process is modeled as a self-avoiding walk (SAW) on  $\mathcal{G}$ , where each amino acid in the sequence occupies a single lattice point, and no two amino acids can occupy the same point simultaneously. The SAW begins by placing the first two amino acids at positions  $\vec{r}_0 = (0, 0, 0)$  and  $\vec{r}_1 = (0, 1, 0)$  in the cubic lattice. The following constraints are imposed on the placement of subsequent amino acids:

- **Distance constraint:** The distance between consecutive amino acids in the sequence must be exactly one lattice unit. Let  $\vec{r}_i = (x_i, y_i, z_i)$  and  $\vec{r}_{i+1} = (x_{i+1}, y_{i+1}, z_{i+1})$  be the positions of two consecutive amino acids. Then, the distance constraint can be expressed as:

$$\|\vec{r}_{i+1} - \vec{r}_i\| = \left( (x_{i+1} - x_i)^2 + (y_{i+1} - y_i)^2 + (z_{i+1} - z_i)^2 \right)^{\frac{1}{2}} = 1 \quad (1)$$

- **Bond angle constraint:** The bond angles formed by three consecutive amino acids must be restricted to  $90^\circ$  or  $180^\circ$  to ensure rotational invariance. Let  $\vec{r}_i, \vec{r}_{i+1}$ , and  $\vec{r}_{i+2}$  be the positions of three consecutive amino acids. The bond angle constraint can be expressed as:

$$\begin{aligned} (\vec{r}_{i+1} - \vec{r}_i) \cdot (\vec{r}_{i+2} - \vec{r}_{i+1}) &= 0 \quad (\text{for a } 90^\circ \text{ angle}) \\ (\vec{r}_{i+1} - \vec{r}_i) \times (\vec{r}_{i+2} - \vec{r}_{i+1}) &= \vec{0} \quad (\text{for a } 180^\circ \text{ angle}) \end{aligned} \quad (2)$$

where  $\cdot$  denotes the dot product and  $\times$  denotes the cross product.

- **Self-avoidance constraint:** The chain must not intersect with itself, i.e., no two amino acids can occupy the same lattice point. This can be expressed as:

$$\vec{r}_i \neq \vec{r}_j \quad \forall i, j \in 0, 1, \dots, N-1, i \neq j \quad (3)$$

where  $N$  is the total number of amino acids in the sequence.

- **Translational invariance:** Translational invariance is ensured by the presence of primitive translation vectors  $(\vec{a}_1, \vec{a}_2, \vec{a}_3)$  that map the lattice onto itself. The translation vectors are defined as:

$$\vec{T} = n_1 \vec{a}_1 + n_2 \vec{a}_2 + n_3 \vec{a}_3 \quad (4)$$

where  $n_1, n_2, n_3 \in \mathbb{Z}$ .

In this problem, the objective is to find the optimal conformation that maximizes the number of hydrophobic-hydrophobic (H-H) contacts in the folded protein. An H-H contact occurs when two non-consecutive hydrophobic amino acids are placed adjacent to each other in the lattice. The energy of a given fold is defined as the negative of the total number of valid H-H contacts:

$$E = -(\text{number of valid H-H contacts}) \quad (5)$$

By minimizing the energy function, the most stable conformation with the maximum number of H-H contacts can be found.

### 2.2 DRL Setup

By treating the protein folding process as a SAW, the RL agent places the amino acids sequentially. In our setup, the protein is considered the agent, and the cubic lattice represents the environment. The length of the path corresponds to the number of amino acids in the protein sequence. At the end of each episode, the environment provides the agent with a reward based on the energy of the achieved fold.

### 2.2.1 Markov Decision Process Formulation

A MDP is defined by a tuple  $(\mathcal{S}, \mathcal{A}, \mathcal{P}, \mathcal{R}, \gamma)$ , where  $\mathcal{S}$  is the state space,  $\mathcal{A}$  is the action space,  $\mathcal{P}$  is the transition probability function,  $\mathcal{R}$  is the reward function, and  $\gamma \in [0, 1]$  is the discount factor. At each discrete time step  $t$ , the agent interacts with the environment by observing the current state  $s_t \in \mathcal{S}$  and taking an action  $a_t \in \mathcal{A}$ . The environment then transitions to a new state  $s_{t+1} \in \mathcal{S}$  according to the transition probability function  $\mathcal{P}(s_{t+1}|s_t, a_t)$  and provides a reward  $r_{t+1} \in \mathcal{R}$  to the agent. The objective of the agent is to learn a policy  $\pi : \mathcal{S} \rightarrow \mathcal{A}$  that maximizes the expected cumulative reward over an episode, defined as  $\mathbb{E} \left[ \sum_{t=0}^T \gamma^t r_t \right]$ , where  $T$  is the length of the episode.

### 2.2.2 Deep Q-Learning with Stabilization Techniques

Deep Q-learning (DQN) is a reinforcement learning algorithm that combines Q-learning with deep neural networks to optimize the conformations achieved by the agent in the protein folding problem. Q-learning is a value-based method that learns the optimal action-value function, or Q-function, which represents the expected future reward for taking a particular action in a given state. The Q-function, denoted as  $Q(s, a)$ , satisfies the Bellman optimality equation:

$$Q(s, a) = \mathbb{E} \left[ r_{t+1} + \gamma \max_{a_{t+1}} Q(s_{t+1}, a_{t+1}) \right] \quad (6)$$

where  $r_{t+1}$  is the reward received at time step  $t + 1$  for carrying out action  $a_t$  at state  $s_t$ ,  $\gamma \in [0, 1]$  is the discount factor that determines the importance of future rewards, and  $s_{t+1}$  is the state at time step  $t + 1$ . The expectation  $\mathbb{E}$  is taken over all possible next states and actions, reflecting the average outcome based on the agent’s policy and the environment’s dynamics. The optimal Q-function, denoted as  $Q^*(s, a)$ , satisfies the Bellman optimality equation and provides the maximum expected future reward for taking action  $a$  in state  $s$ . DQN addresses the limitations of traditional Q-learning, which becomes intractable for problems with large state spaces, by approximating the Q-function using a deep neural network. The neural network, parameterized by  $\theta$ , takes the state  $s$  as input and outputs the Q-values for each action  $a$ . The training objective is to minimize the mean-squared error loss function:

$$\mathcal{L}(\theta) = \mathbb{E} \left[ \left( r + \gamma \max_{a_{t+1}} Q(s_{t+1}, a_{t+1}; \theta^-) - Q(s, a; \theta) \right)^2 \right] \quad (7)$$

where  $s_{t+1}$  is the next state,  $a_{t+1}$  is the next action, and  $\theta^-$  represents the parameters of a target network. The target network is a separate neural network that is periodically updated with the parameters of the main network, denoted as  $\theta$ . The use of a target network is a key stabilization technique introduced in the DQN paper by [Mnih et al., 2015], which helps to mitigate the issue of divergence in the learning process. During training, the agent interacts with the environment and stores the experienced transitions  $e_t = (s_t, a_t, r_{t+1}, s_{t+1})$  in a replay buffer  $\mathcal{D}$ . The replay buffer is a fixed-size cache that stores the most recent transitions experienced by the agent. At each training step, a minibatch of transitions  $e_1, e_2, \dots, e_N$  is sampled uniformly from the replay buffer to update the parameters of the main network  $\theta$ . The use of a replay buffer helps to break the correlation between consecutive samples and stabilizes the learning process by providing a diverse set of experiences for training.

The training process is displayed in Figure 1 and proceeds as follows:

1. Sample a minibatch of transitions  $e_1, e_2, \dots, e_N$  from the replay buffer  $\mathcal{D}$ .
2. For each transition  $e_t = (s_t, a_t, r_{t+1}, s_{t+1})$ , compute the target:

$$y_t = \begin{cases} r_{t+1} & \text{if } s_{t+1} \text{ is terminal} \\ r_{t+1} + \gamma \max_{a'} Q(s_{t+1}, a'; \theta^-) & \text{otherwise} \end{cases} \quad (8)$$

3. Update the parameters  $\theta$  of the main network by minimizing the loss function:

$$\mathcal{L}(\theta) = \frac{1}{N} \sum_{t=1}^N (y_t - Q(s_t, a_t; \theta))^2 \quad (9)$$

4. Every  $C$  steps, update the parameters  $\theta^-$  of the target network by copying the parameters  $\theta$  of the main network:

$$\theta^- \leftarrow \theta \quad (10)$$

5. Select an action  $a_t$  based on the current state  $s_t$  using an  $\epsilon$ -greedy policy derived from the Q-values:

$$a_t = \begin{cases} \operatorname{argmax} Q(s_t, a; \theta) & \text{with probability } 1 - \epsilon \\ \text{random action} & \text{with probability } \epsilon \end{cases} \quad (11)$$

where  $\epsilon$  is the exploration rate that determines the probability of selecting a random action instead of the greedy action with the highest Q-value.

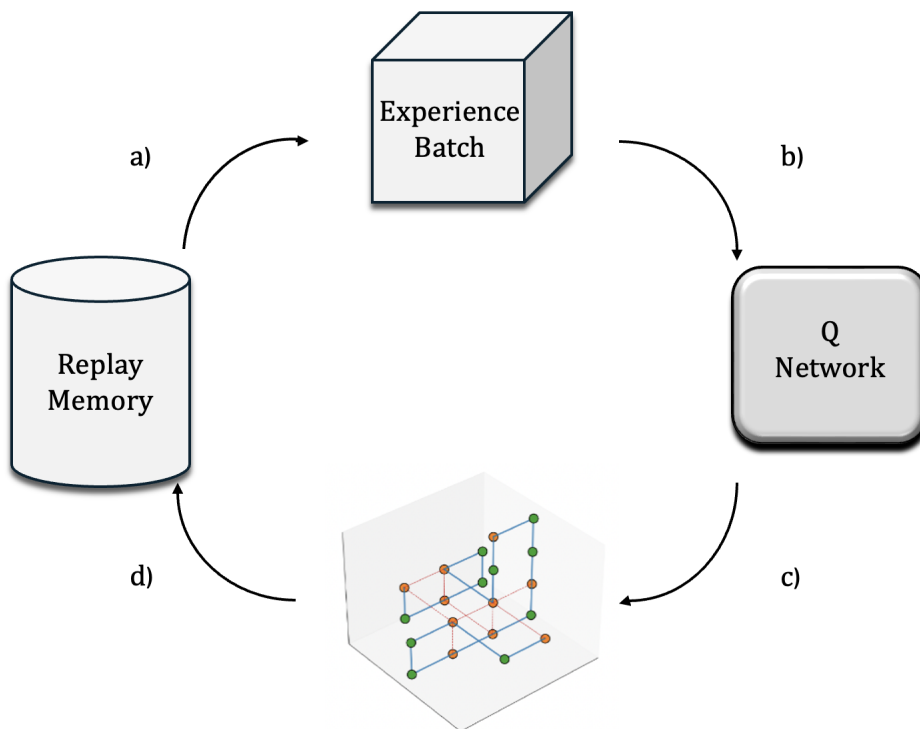


Figure 1: Deep reinforcement learning training loop. In a), we sample a batch of experience from the buffer. The batch then serves as input to the Q - network in b). Based on the output Q - value tensor, the agent makes a decision in c) to take  $a_{t+1}$  that corresponds to the greatest value of the Q - output tensor. In step d), the experience is stored in the replay memory..

6. Execute the selected action  $a_t$  in the environment and observe the next state  $s_{t+1}$  and reward  $r_{t+1}$ .
7. Store the transition  $(s_t, a_t, r_{t+1}, s_{t+1})$  in the replay buffer  $\mathcal{D}$ .

### 2.2.3 State Representation

We represent the states using one-hot encoded vectors. Each state vector consists of two parts: the first part represents the available actions (forward (F), backward (B), right (R), left (L), up (U), and down (D)), and the second part encodes the type of amino acid (H or P) at the current position. Specifically, the state is an 8-dimensional vector, where the first six elements correspond to the possible actions the agent can take: No Decision (ND), F, L, R, U, D. The last two elements represent the type of amino acid (H or P). For each training episode, we obtain a 3D shape tensor  $(N, 8, 1)$ , where  $N$  is the length of the protein sequence. The first dimension corresponds to the time steps, that is, the positions in the protein sequence, while the second dimension represents the state features (actions and amino acid type). The third dimension is a singleton dimension to facilitate input to the neural network. This state representation allows the agent to make informed decisions based on the available actions and the type of amino acid at each position. By concatenating action and amino acid information, the neural network can learn the dependencies between amino acid placements and the resulting energy conformations. It is important to note that the neural network does not directly observe amino acid placements; instead, it deduces this information from actions taken thus far. The “No Decision” (ND) indicates a state where no further moves are possible, leading to episode termination. The backward action (B) is excluded because once an amino acid is placed at a position, revisiting that position is not feasible; thus, it cannot be performed in this context.

### 2.3 Q - Network Architectures

In this subsection, we describe the two architectures proposed in this paper.

### 2.3.1 Hybrid - Reservoir

The architecture consists of a reservoir layer followed by several fully connected layers, as illustrated in Figure 2.

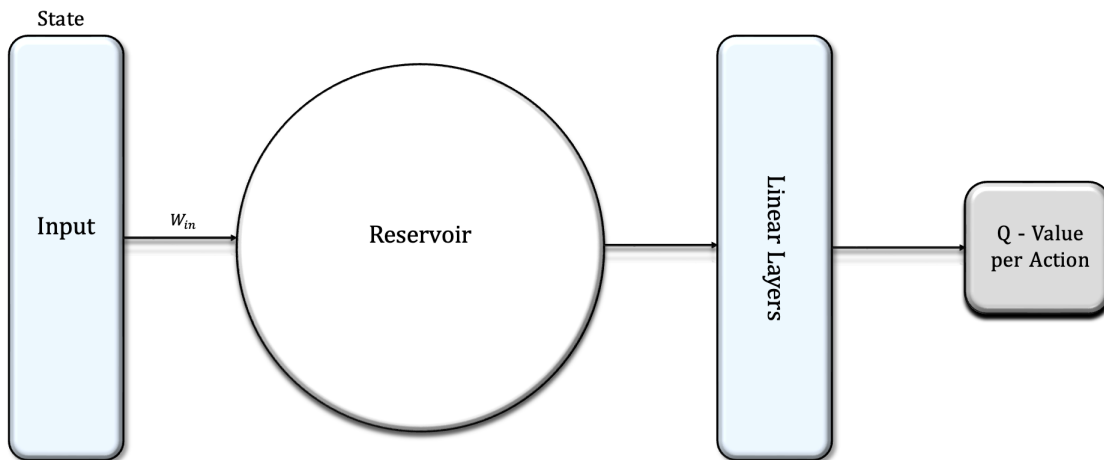


Figure 2: The input layer consists of a  $(N, 8, 1)$  tensor representing the state at a particular timestep. The reservoir is a randomly initialized weight matrix with a topology specified beforehand. The linear layers consists of a simple fully-connected feed forward neural network. The output is a  $(5, 1)$  tensor representing the Q - value or future expected total reward per action.

The input to the reservoir neural network is a flattened vector representation of the state, denoted as  $\mathbf{x} \in \mathbb{R}^{N \times d}$ , where  $N$  is the sequence length and  $d$  is the dimensionality of the one-hot encoded vector described in 2.2.3. The reservoir layer applies a fixed random projection of the input into a high-dimensional space. Mathematically, the reservoir layer can be described as follows:

$$\mathbf{r}(t) = f(\mathbf{W}_{in}\mathbf{x}(t) + \mathbf{W}\mathbf{r}(t-1)) \quad (12)$$

where  $\mathbf{r}(t) \in \mathbb{R}^{N_r}$  is the reservoir state at time step  $t$ ,  $\mathbf{x}(t) \in \mathbb{R}^d$  is the input state,  $\mathbf{W}_{in} \in \mathbb{R}^{N_r \times d}$  is the trainable input weight matrix,  $\mathbf{W} \in \mathbb{R}^{N_r \times N_r}$  is the reservoir weight matrix, and  $f(\cdot)$  is the activation function (e.g., hyperbolic tangent). The reservoir weight matrix  $\mathbf{W}$  is randomly initialized and remains fixed during training. It follows a specific connectivity pattern, such as the Erdős-Rényi topology, which promotes a limited number of active connections among neurons. The sparsity and connectivity of the reservoir are important factors in determining its computational capacity and ability to capture complex dynamics. The size of the reservoir, denoted as  $N_r$ , is a hyperparameter that depends on the length and complexity of the protein sequence. Empirically, we found that a reservoir size of 1000 works well for sequences of length  $N \leq 36$ , while for longer sequences ( $N = 48, 50$ ), a larger reservoir size of around 3000 is used to capture the increased complexity. The reservoir layer applies a hyperbolic tangent (tanh) activation function to introduce nonlinearity. The output of the reservoir layer is then passed through a series of fully connected layers with Rectified Linear Unit (ReLU) activation functions. The sizes of the fully connected layers are 512, 256, 128, and 84, respectively. These layers learn to extract meaningful features from the reservoir representation and progressively reduce the dimensionality of the feature space. The final output layer is a fully connected layer with a size equal to the number of actions, which generates the Q-values for each action.

### 2.3.2 LSTM with Multi-Head-Attention

For long proteins, we employ an LSTM architecture with multi-head attention [Vaswani et al., 2017]. The architecture consists of an LSTM layer, a multi-head attention mechanism, and a fully connected output layer, as illustrated in Figure 3.

The multi-head attention mechanism enhances the network’s ability to focus on different aspects of the input sequence simultaneously. Given an input sequence processed by the LSTM layers producing hidden states  $\mathbf{H} \in \mathbb{R}^{N \times d}$ , where  $N$  is the sequence length and  $d$  is the hidden dimension, the attention mechanism computes attention patterns across four different representation subspaces. For each attention head  $i$ , the mechanism computes:

$$\text{Attention}_i(\mathbf{Q}, \mathbf{K}, \mathbf{V}) = \text{softmax} \left( \frac{\mathbf{Q}\mathbf{K}^T}{\sqrt{d_k}} \right) \mathbf{V} \quad (13)$$

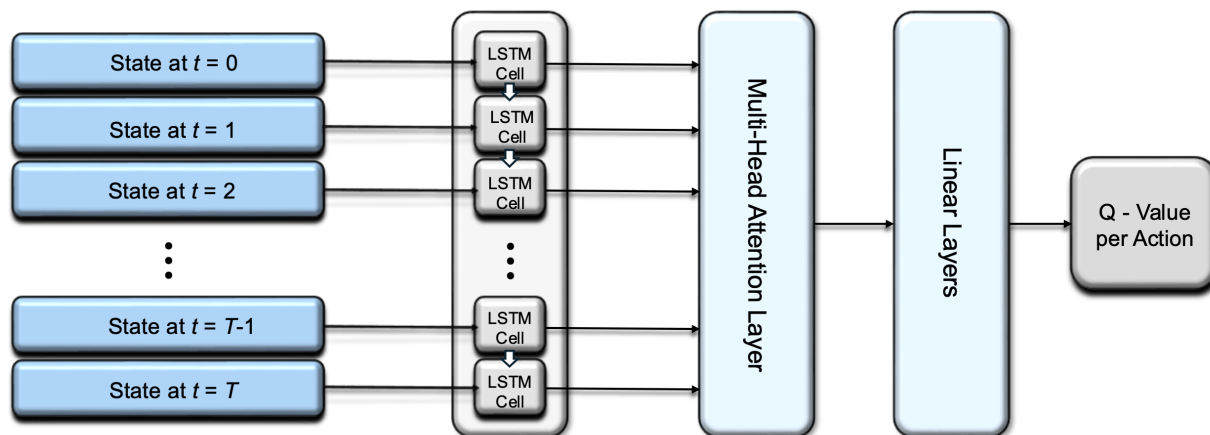


Figure 3: LSTM-A architecture for protein folding. Sequential states are processed through LSTM cells, generating hidden states that are weighted by an 8-head attention mechanism. The attention output is mapped to action Q-values through a fully connected layer, enabling the model to leverage both sequential patterns and long-range dependencies.

where  $\mathbf{Q}$ ,  $\mathbf{K}$ , and  $\mathbf{V}$  are linear projections of the LSTM output  $\mathbf{H}$ , and  $d_k$  is the dimension of the key vectors. The outputs from all heads are concatenated and projected to the required dimension using a weight matrix  $\mathbf{W}^O$ :

$$\text{MultiHead}(\mathbf{H}) = \text{Concat}(\text{head}_1, \dots, \text{head}_4) \mathbf{W}^O \quad (14)$$

Our implementation uses a hidden size of  $d = 512$  with four attention heads. The LSTM layer processes the input sequence with batch-first ordering, and the attention mechanism operates on the full sequence of LSTM outputs. The final output is obtained by selecting the last time step of the attention output, followed by a fully connected layer that maps to the action space dimension.

### 3 Experiments and Results

To evaluate our approach, we utilized sequences with best-known energy values published in Table 1 from [Boumedine and Bouroubi, 2022]. Figure 4 illustrates the optimal folds for various sequences, providing a benchmark for our experiments. We began our investigation with the baseline Fully Connected Feedforward Neural Network (FFNN), which employs a four-layer architecture (512→256→84→output-size) with ReLU activations. This model was effective for shorter sequences ( $N \leq 36$ ), demonstrating reasonable performance in achieving optimal energy states. However, it struggled with longer sequences, often failing to converge to the best-known values for more complex protein structures. This limitation highlighted the need for enhancements that could better capture the intricate dynamics of protein folding. To address these shortcomings, we introduced the Reservoir-based Fully Connected Feedforward Neural Network (FFNN-R). By incorporating a reservoir layer initialized using Xavier uniform initialization and tanh activation, FFNN-R enhanced the network’s temporal memory capabilities while maintaining training efficiency. The reservoir’s sparsity and specific connectivity patterns allowed for improved processing of input data. Empirical results showed that FFNN-R outperformed the vanilla FFNN, converging to optimal energy states faster, requiring approximately 25% fewer training episodes to reach these conformations. Particularly for shorter sequences, FFNN-R consistently achieved BKVs for sequences A1-A5 and A8-A10, showcasing its superior convergence speed. Building on the improvements seen with FFNN-R, we explored LSTM architectures to further enhance performance on longer sequences. The LSTM-OLH architecture utilized traditional LSTM cells while relying solely on the last hidden state for decision-making. While this approach provided some improvements over FFNN, it still struggled to effectively capture long-range dependencies critical in protein folding. To maximize performance further, we developed the LSTM-A architecture, which incorporated a multi-head attention mechanism. This enhancement allowed the model to dynamically weigh different temporal aspects of the state sequence, effectively capturing long-range interactions between amino acids. The results indicated that LSTM-A significantly outperformed both LSTM-OLH and vanilla FFNN implementations for longer sequences ( $N > 36$ ). It consistently achieved optimal or near-optimal energy states that matched BKVs for sequences 3d1-3d5 and approached BKVs for more challenging sequences like 3d6-3d9. Throughout our experiments, we employed a stabilized Deep Q-Learning framework with experience replay and an epsilon-greedy strategy for action selection. The training utilized a single NVIDIA H100 GPU with architectures

implemented in PyTorch version 2.5.0 running on CUDA version 11.8. The Adam optimizer was used with a learning rate of 0.001, and we selected the smooth L1 loss function for its effectiveness in DQL tasks with discrete action spaces. As shown in Figure 5, for shorter sequences ( $N \leq 36$ ), FFNN-R outperformed other architectures and converged to optimal energy states more rapidly. However, for longer sequences, LSTM-A exhibited superior performance compared to both LSTM-OLH and vanilla FFNN implementations. The training process revealed that the attention mechanism in LSTM-A began to play a crucial role after approximately 100,000 training episodes, coinciding with significant improvements in energy minimization. This suggests that the network first learns local folding patterns before leveraging attention to capture long-range dependencies. In contrast, the FFNN-R architecture demonstrated rapid initial convergence, often reaching near-optimal conformations within the first 50,000 episodes, particularly for shorter sequences. Moreover, FFNN-R provided more efficient parameter utilization as it required only 264,445 trainable parameters compared to LSTM-A's 6,324,741. In summary, our findings illustrate a clear progression in model performance from vanilla FFNN to reservoir-based architectures and finally to LSTM networks with attention mechanisms. Each architectural enhancement addressed specific challenges in protein folding prediction, culminating in models that not only achieved optimal conformations but also demonstrated improved training efficiency across varying sequence lengths.

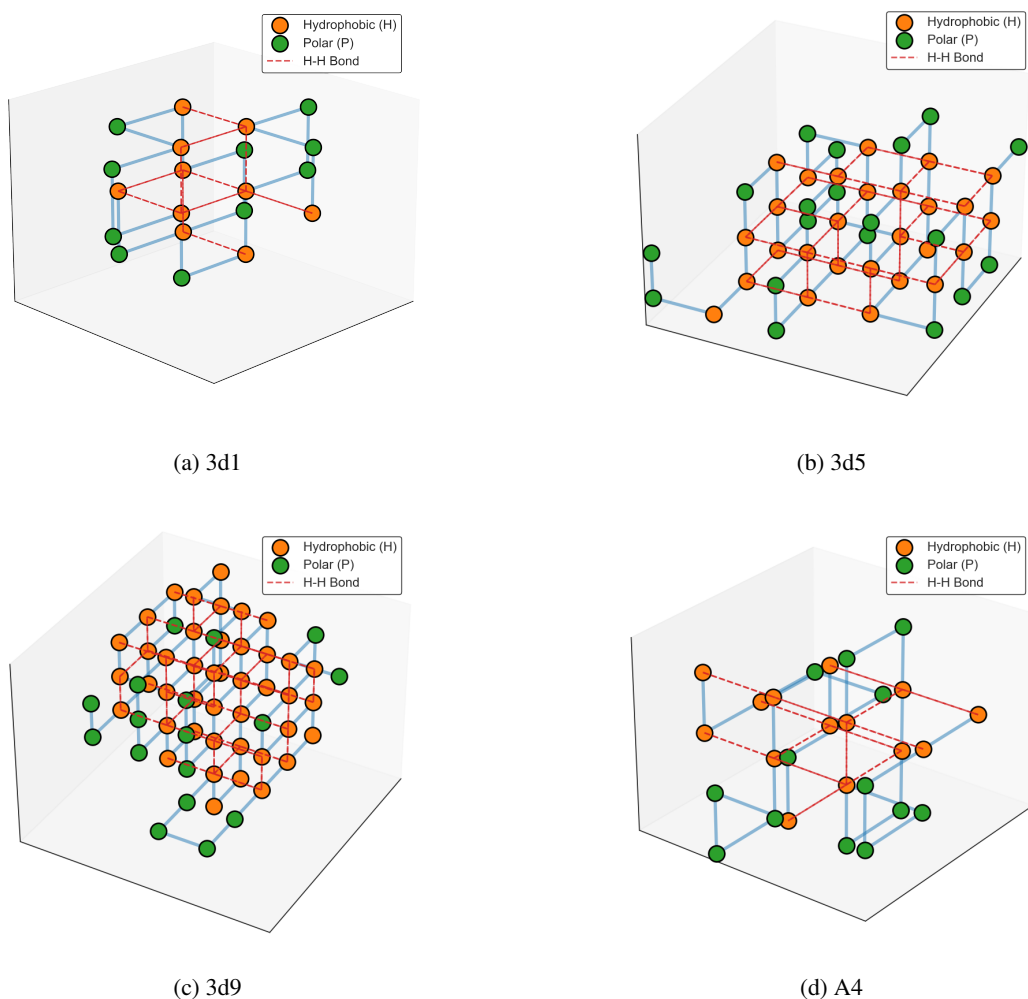


Figure 4: Least Energy Conformations for different sequences.

### 3.1 Efficiency

The LSTM-A and FFNN-R architectures demonstrate distinct computational profiles in memory usage and training efficiency. LSTM-A requires 2.4GB memory for sequences  $\leq 36$  residues (3d1-3d4), with memory distributed across LSTM layers (512 units, 1.8GB), multi-head attention mechanism (0.4GB), and auxiliary layers (0.2GB). FFNN-R

Table 1: Sequences and their corresponding best known conformation energy values (BKV).

SEQ.	LENGTH	SEQUENCE	BKV
3D1	20	$(HP)^2PH(HP)^2(PH)^2HP(PH)^2$	-11
3D2	24	$H^2P^2(HP^2)^6H^2$	-13
3D3	25	$P^2HP^2(H^2P^4)^3H^2$	-9
3D4	36	$P(P^2H^2)^2P^5H^5(H^2P^2)^2P^2H(HP^2)^2$	-18
3D5	46	$P^2H^3PH^3P^3HPH^2PH^2P^2HPH^4$ $PHP^2H^5PHPH^2P^2H^2P$	-35
3D6	48	$P^2H(P^2H^2)^2P^5H^{10}P^6$ $(H^2P^2)^2HP^2H^5$	-31
3D7	50	$H^2(PH)^3PH^4PH(P^3H)^2P^4$ $(HP^3)^2HPH^4(PH)^3PH^2$	-34
3D8	58	$PH(PH^3)^2P(PH^2PH)^2H(HP)^3$ $(H^2P^2H)^2PHP^4(H(P^2H)^2)^2$	-44
3D9	60	$P(PH^3)^3H^5P^3H^{10}PHP^3$ $H^{12}P^4H^6PH^2PH$	-55

Table 2: Sequences and their corresponding best known conformation energy values (BKV) (continued).

SEQ.	LENGTH	SEQUENCE	BKV
A <sub>1</sub>	27	$PHPHPH^3P^2HPHP^{11}H^2P$	-9
A <sub>2</sub>	27	$PH^2P^{10}H^2P^2H^2P^2HP^2HPH$	-10
A <sub>3</sub>	27	$H^4P^5HP^4H^3P^9H$	-8
A <sub>4</sub>	27	$H^3P^2H^4P^3HPHP^2H^2P^2HP^3H^2$	-15
A <sub>5</sub>	27	$H^4P^4HPH^2P^3H^2P^{10}$	-8
A <sub>6</sub>	27	$HP^6HPH^3P^2H^2P^3HP^4HPH$	-12
A <sub>7</sub>	27	$HP^2HPH^2P^3HP^5HPH^2PHPHPH^2$	-13
A <sub>8</sub>	27	$HP^{11}HPHP^8HPH^2$	-4
A <sub>9</sub>	27	$P^7H^3P^3HPH^2P^3HP^2HP^3$	-7
A <sub>10</sub>	27	$P^5H^2PHPHPHPH^2H^2PH^2PH^3$	-11
A <sub>11</sub>	27	$HP^4H^4P^2HPHPH^3PHP^2H^2P^2H$	-16

maintains a consistent 800MB footprint, comprising a sparse reservoir (1000 nodes, 10% connectivity, 400KB), input weights (1000 × 8, 32KB), and fully connected layers (256 and 84 nodes, 1MB), with remaining memory allocated to batch processing and gradients. Training performance reveals significant differences between architectures. LSTM-A requires 500,000 episodes for optimal convergence on longer sequences (48-50 residues), with training times averaging 8 hours for sequences ≤ 36 and extending to 48 hours for sequences 3d5-3d9. In contrast, FFNN-R achieves convergence in approximately 200,000 episodes for shorter sequences (≤ 36 residues), completing training in 1.5 hours. FFNN-R’s reservoir demonstrates efficient exploration, achieving 80-90% unique conformational states within the first 50,000 episodes before focusing on promising conformations. LSTM-A compensates for its higher computational demands through parallel processing via its multi-head attention mechanism, enabling efficient handling of longer sequences while reducing computational bottlenecks.

## 4 Discussion

Our analysis reveals several key insights into both architectures’ effectiveness. The LSTM-A’s 4-head attention mechanism proves optimal for capturing long-range dependencies in protein folding, as evidenced by the attention weight patterns shown in Figure 7. The visualization demonstrates how different attention heads specialize over training iterations – initially showing uniform weights (yellow matrices) that evolve into distinct patterns capturing both local and global protein structure interactions. Network depth beyond 5 layers shows a decrease in performance, while batch size of 32 provides optimal balance between memory usage and training stability.

Compared to traditional genetic algorithms and Monte Carlo methods, the LSTM-A demonstrates superior performance on longer sequences while requiring significantly less computational time to reach optimal conformations. The evolution



Table 3: Energy values of 3d protein sequences obtained by different algorithms. The right-most column corresponds to the least energy conformation found by our models. The results of all experiments tabulated in Table 4 in the appendix section.

SEQ.	LENGTH	BKV	GA	BILS	LSTM-A
3D1	20	<b>-11</b>	-11	-10	-11
3D2	24	<b>-13</b>	-13	-9	-13
3D3	25	<b>-9</b>	-9	-7	-9
3D4	36	<b>-18</b>	-18	-12	-18
3D5	46	<b>-35</b>	-32	-22	-33
3D6	48	<b>-31</b>	-31	-19	-30
3D7	50	<b>-34</b>	-30	-18	-32
3D8	58	<b>-44</b>	-37	-23	-40
3D9	60	<b>-55</b>	-50	-36	-51

SEQ.	LENGTH	BKV	GA	TPPSO	FFNN-R
A <sub>1</sub>	27	<b>-9</b>	-8	-9	-9
A <sub>2</sub>	27	<b>-10</b>	-10	-10	-10
A <sub>3</sub>	27	<b>-8</b>	NA	-8	-8
A <sub>4</sub>	27	<b>-15</b>	-15	-15	-15
A <sub>5</sub>	27	<b>-8</b>	-8	-8	-8
A <sub>6</sub>	27	<b>-12</b>	NA	-11	-11
A <sub>7</sub>	27	<b>-13</b>	-13	-12	-12
A <sub>8</sub>	27	<b>-4</b>	-4	-4	-4
A <sub>9</sub>	27	<b>-7</b>	-7	-7	-7
A <sub>10</sub>	27	<b>-11</b>	NA	-11	-11

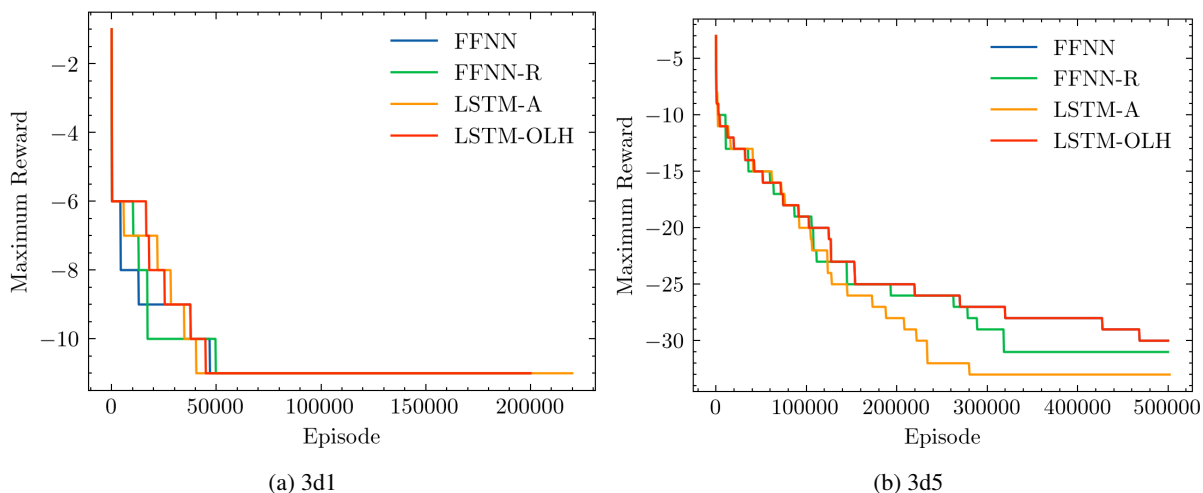


Figure 5: Plots a) 3d1 and b) 3d5 show the minimum conformation energy as a function of episode.

of attention weights in Figure 7 reveals how Head 1 develops periodic patterns suggesting secondary structure detection, while Head 2 shows strong position-specific interactions through deeper blue-green regions. Heads 3 and 4 capture broader contextual patterns with more diffuse attention distribution, enabling the model to simultaneously process both local and long-range amino acid interactions.

The FFNN-R’s success relies on its 1000-neuron reservoir for sequences up to length 36, with linear scaling required for longer sequences. The reservoir’s ability to implicitly model temporal dependencies allows the network to capture essential folding patterns without explicit recurrent connections, contributing to its computational efficiency. When compared to traditional FFNN and hybrid approaches like BILS, the FFNN-R shows faster convergence and better energy minimization for shorter sequences. Both FFNN and FFNN-R demonstrate robust performance across multiple independent training runs. While traditional approaches like ant colony optimization and pruned-enriched Rosenbluth

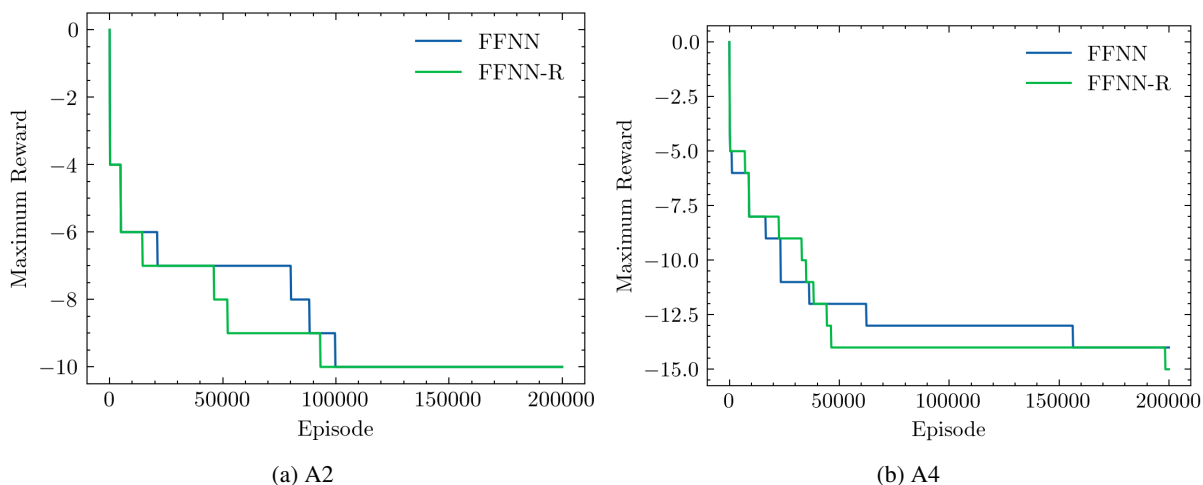


Figure 6: Plots a) A2 and b) A4 show the minimum conformation energy as a function of episode.

method often require multiple restarts to achieve optimal results, our architectures show consistent performance with lower variance in final energy values.

However, several important limitations emerge at scale. LSTM-A training becomes computationally demanding beyond 60 amino acids, while FFNN-R performance degrades significantly after length 36. Memory requirements for LSTM-A scale quadratically with sequence length, potentially limiting application to very long sequences. The performance on benchmark sequences suggests both architectures capture fundamental principles of protein folding within the HP model. The LSTM-A’s success on longer sequences indicates effective modeling of the hierarchical nature of protein folding, where local structures form first and then assemble into global conformations, as demonstrated by the progressive specialization of attention heads in Figure 7. The FFNN-R’s efficiency on shorter sequences suggests rapid learning of local interactions, often sufficient for determining smaller protein structures, providing a more efficient alternative to traditional Monte Carlo sampling approaches.

When compared to core-directed chain growth methods and hybrid evolutionary algorithms, both LSTM-A and FFNN-R show comparable or superior performance in terms of final energy values while requiring less parameter tuning and fewer computational resources. The attention mechanism in LSTM-A particularly excels at capturing the kind of long-range interactions that traditional methods often struggle to model effectively, with the attention weights visualization in Figure 7 showing clear evidence of the model learning to focus on both local structural motifs and distant amino acid interactions during training.

#### 4.1 Limitations and Future Directions

Our implementation achieves state-of-the-art results for the HP model, though important limitations remain. The reservoir-based approach shows decreased performance for proteins exceeding 36 residues, while the LSTM-A architecture, though more robust for longer sequences, demands substantial computational resources and training time. Future work should address several key challenges: extending the architectures to handle realistic protein force fields, incorporating additional physical constraints, optimizing the attention mechanism’s efficiency for longer sequences, and exploring hybrid approaches that leverage the strengths of both architectures. The linear scaling relationship between sequence length and reservoir size also merits investigation for improved efficiency. The HP model provides an ideal benchmark system, capturing fundamental protein folding aspects while remaining computationally tractable. Its NP-complete nature in finding optimal conformations makes it particularly valuable for testing new algorithms. Notably, our methods successfully achieve optimal conformations that align with known energy minima.

## 5 Conclusion

This study advances protein structure prediction through two novel architectures. The LSTM-A achieves good performance on longer sequences ( $N > 36$ ), while the FFNN-R provides efficient solutions for shorter sequences. Both consistently match best-known energy values across benchmark sequences. The success of these architectures demonstrates the viability of deep learning approaches in protein structure prediction, while establishing new benchmarks for

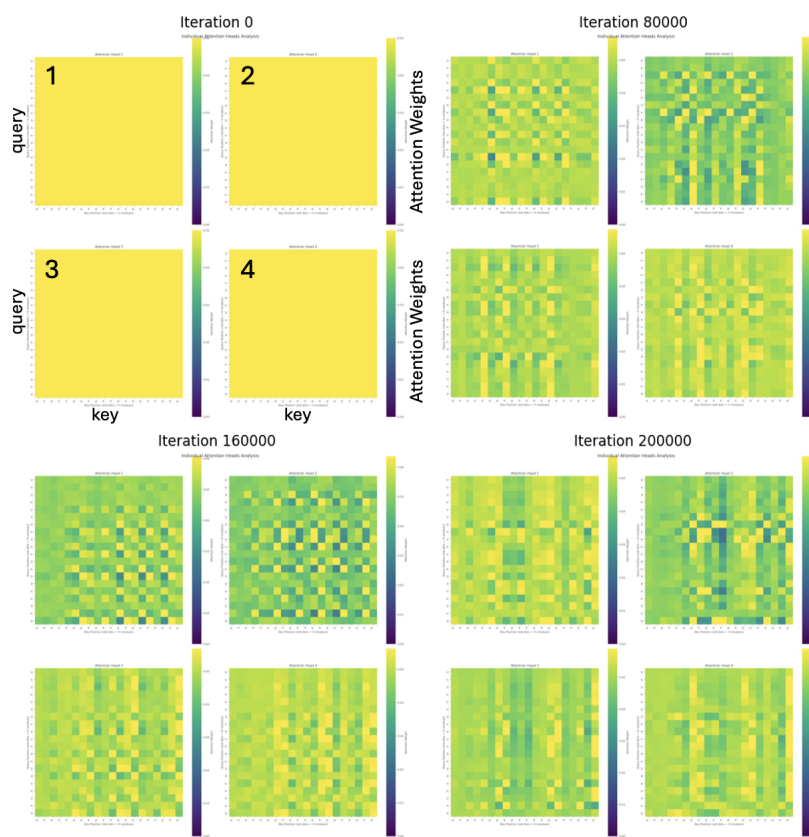


Figure 7: Evolution of multi-head attention weights during protein structure prediction training. Each row shows the attention patterns of four attention heads at different training iterations (0, 80,000, 160,000, and 200,000). The x and y axes represent query and key positions in the protein sequence, with colors indicating attention strength (purple: 0.0 to yellow: 0.05).

computational efficiency. Their complementary strengths suggest promising directions for handling proteins of varying lengths and complexities. Future work should explore hybrid architectures combining LSTM-A and FFNN-R strengths, more efficient attention mechanisms for longer sequences, and parallel training strategies.

## Software and Data

The software and data used in this study are available in a public GitHub repository. This repository contains the implementation of our protein structure prediction model using deep reinforcement learning in the 3D HP model.

## Acknowledgements

This work was supported by the National Institutes of Health (R01-GM148586). Simulations were run on the Hive cluster, which is supported by the National Science Foundation under grant number 1828187, and the Phoenix cluster, both of which are managed by the Partnership for an Advanced Computing Environment (PACE) at the Georgia Institute of Technology.

## References

E. A. Antonelo and B. Schrauwen. On learning navigation behaviors for small mobile robots with reservoir computing architectures. *IEEE Trans. Neural Netw. Learn. Syst.*, 26(4):763–780, 4 2015. doi: 10.1109/tnnls.2014.2323247.

- F. A. Araujo, M. Riou, J. Torrejon, S. Tsunegi, D. Querlioz, K. Yakushiji, A. Fukushima, H. Kubota, S. Yuasa, M. D. Stiles, and J. Grollier. Role of non-linear data processing on speech recognition task in the framework of reservoir computing. *Sci. Rep.*, 10(1), 1 2020. doi: 10.1038/s41598-019-56991-x.
- D. Bahdanau, K. Cho, and Y. Bengio. Neural machine translation by jointly learning to align and translate. *arXiv*, 1 2015.
- T. C. Beutler and K. A. Dill. A fast conformational search strategy for finding low energy structures of model proteins. *Protein Sci.*, 5(10):2037–2043, 10 1996. doi: 10.1002/pro.5560051010.
- N. Boumedine and S. Bouroubi. Protein folding in 3D lattice HP model using a combining cuckoo search with the Hill-Climbing algorithms. *Appl. Soft Comput.*, 119:108564, 4 2022. doi: 10.1016/j.asoc.2022.108564.
- G. Czibula, M.-I. Bocicor, and I.-G. Czibula. Solving the protein folding problem using a distributed Q-Learning approach. Technical Report 3, Babeş-Bolyai Univ., 2011.
- B. Doğan and T. Ölmez. A novel state space representation for the solution of 2D-HP protein folding problem using reinforcement learning methods. *Appl. Soft Comput.*, 26:213–223, 1 2015. doi: 10.1016/j.asoc.2014.09.047.
- P. Grassberger. Pruned-enriched Rosenbluth method: Simulations of  $\theta$  polymers of chain length up to 1 000 000. *Phys. Rev. E*, 56(3):3682–3693, 9 1997. doi: 10.1103/physreve.56.3682.
- H. Jaeger. Echo state network. *Scholarpedia*, 2(9):2330, 1 2007. doi: 10.4249/scholarpedia.2330.
- N. Krasnogor. Studies on the theory and design space of memetic algorithms. *PhD Thesis*, 6 2010.
- Y. Li, H. Kang, K. Ye, S. Yin, and X. Li. FoldingZero: Protein Folding from Scratch in Hydrophobic-Polar Model. *Neural Inf. Process. Syst.*, 12 2018.
- V. Mnih, K. Kavukcuoglu, D. Silver, A. A. Rusu, J. Veness, M. G. Bellemare, A. Graves, M. Riedmiller, A. K. Fidjeland, G. Ostrovski, S. Petersen, C. Beattie, A. Sadik, I. Antonoglou, H. King, D. Kumaran, D. Wierstra, S. Legg, and D. Hassabis. Human-level control through deep reinforcement learning. *Nature*, 518(7540):529–533, 2 2015. doi: 10.1038/nature14236.
- A. L. Patton, W. F. Punch, and E. D. Goodman. A standard GA approach to native protein conformation prediction. *Int. Conf. Genet. Algorithms*, pages 574–581, 7 1995.
- A. Shmygelska and H. H. Hoos. An ant colony optimisation algorithm for the 2D and 3D hydrophobic polar protein folding problem. *BMC Bioinformatics*, 6(1), 2 2005. doi: 10.1186/1471-2105-6-30.
- A. Subramoney, F. Scherr, and W. Maass. *Reservoirs learn to learn*. 1 2021. doi: 10.1007/978-981-13-1687-6\_3.
- R. Unger and J. Moult. Genetic algorithms for protein folding simulations. *J. Mol. Biol.*, 231(1):75–81, 5 1993. doi: 10.1006/jmbi.1993.1258.
- A. Vaswani, N. Shazeer, N. Parmar, J. Uszkoreit, L. Jones, A. N. Gomez, L. Kaiser, and I. Polosukhin. Attention is All you Need. *arXiv*, 30:5998–6008, 6 2017.
- K. Yang, H. Huang, O. Vandans, A. Murali, F. Tian, R. H. C. Yap, and L. Dai. Applying deep reinforcement learning to the HP model for protein structure prediction. *Physica A*, 609:128395, 1 2023. doi: 10.1016/j.physa.2022.128395.

## A Experiments

All of the conducted experiments are tabulated in Table A.1.

Table A.1: 3D Trial Runs, Dictionary: LSTM-OLH  $\rightarrow$  LSTM - OnlyLastHidden, LSTM-A (Num of Heads)  $\rightarrow$  LSTM - with Attention, FNN-VANILLA  $\rightarrow$  Without Reservoir, FNN-Reservoir  $\rightarrow$  With Reservoir

Sequence	Architecture	Num Layers	Size of Layer	Batch Size	Num Training Episodes	Time to Train	Date	E_Min Best	E_min Experimental	Num Parameters
3d1	LSTM-A (4)	3	512	16	200K	6:54:38	10/12/24	-11	-11	6324741
3d2	LSTM-A (4)	3	512	16	220K	7:33:33	10/12/24	-13	-13	6324741
3d3	LSTM-A (4)	3	512	16	220K	7:54:00	12/12/24	-9	-9	6324741
3d4	LSTM-A (4)	3	512	16	250K	11:14:39	10/12/24	-18	-18	6324741
3d5	LSTM-A (4)	5	512	16	500K	41:27:15	10/13/24	-35	-33	10527237
3d6	LSTM-A (4)	5	512	16	500K	41:23:16	10/13/24	-31	-30	10527237
3d5	LSTM-A (4)	5	512	32	750K	45:15:55	10/20/24	-35	-33	10527237
3d7	LSTM-A (4)	5	512	32	750K	49:49:49	10/20/24	-34	-32	10527237
3d6	LSTM-A (4)	5	512	32	750K	46:15:23	10/22/24	-31	-30	10527237
3d8	LSTM-A (4)	5	512	32	750K	57:00:00	10/22/24	-44	-40	10527237
3d8	LSTM-A (4)	6	512	32	750K	-	10/22/24	-44	-	-
3d9	LSTM-A (4)	5	512	32	750K	65:00:00	10/26/24	-55	-51	-
3d1	LSTM-OLH	3	512	16	200K	3:18:16	10/26/24	-11	-11	5274117
3d2	LSTM-OLH	3	512	16	220K	4:06:36	10/26/24	-13	-13	5274117
3d3	LSTM-OLH	3	512	16	220K	1:06:10	10/26/24	-9	-9	5274117
3d4	LSTM-OLH	3	512	16	250K	1:24:51	10/26/24	-18	-18	-
3d5	LSTM-OLH	5	512	16	500K	-	10/26/24	-35	-35	-
3d6	LSTM-OLH	5	512	16	500K	-	10/26/24	-	-	-
3d7	LSTM-OLH	5	512	32	750K	-	10/26/24	-	-	-
3d8	LSTM-OLH	5	512	32	750K	-	10/26/24	-	-	-
3d9	LSTM-OLH	5	512	32	750K	-	10/26/24	-	-	-
3d1	FNN-VANILLA	4	512, 256, 84	16	200K	0:58:15	10/26/24	-11	-11	-
3d2	FNN-VANILLA	4	512, 256, 84	16	220K	1:06:16	10/26/24	-13	-13	-
3d3	FNN-VANILLA	4	512, 256, 84	16	220K	1:06:29	10/26/24	-9	-9	-
3d4	FNN-VANILLA	4	512, 256, 84	16	250K	1:25:10	10/26/24	-18	-18	-
3d5	FNN-VANILLA	4	512, 256, 84	16	500K	3:13:46	10/26/24	-35	-30	-
A1	FNN-VANILLA	4	512, 256, 84	16	200K	1:08:39	10/30/24	-9	-9	-
A2	FNN-VANILLA	4	512, 256, 84	16	200K	1:08:18	10/30/24	-10	-10	-
A3	FNN-VANILLA	4	512, 256, 84	16	200K	1:26:09	10/30/24	-8	-8	-
A4	FNN-VANILLA	4	512, 256, 84	16	200K	1:27:57	10/30/24	-15	-14	-
A5	FNN-VANILLA	4	512, 256, 84	16	200K	-	10/30/24	-8	-8	-
A6	FNN-VANILLA	4	512, 256, 84	16	200K	1:09:17	10/30/24	-12	-11	-
A7	FNN-VANILLA	4	512, 256, 84	16	200K	1:27:20	10/30/24	-13	-12	-
A8	FNN-VANILLA	4	512, 256, 84	16	200K	1:27:26	10/30/24	-4	-4	-
A9	FNN-VANILLA	4	512, 256, 84	16	200K	1:27:50	10/30/24	-7	-6	-
A10	FNN-VANILLA	4	512, 256, 84	16	200K	1:27:57	10/30/24	-11	-11	-
A1	FNN-RESERVOIR	4	512, 256, 84	16	200K	1:12:23	11/2/2024	-9	-9	264445
A2	FNN-RESERVOIR	4	512, 256, 84	16	200K	1:27:59	11/2/2024	-10	-10	-
A3	FNN-RESERVOIR	4	512, 256, 84	16	200K	1:13:31	11/2/2024	-8	-8	-
A4	FNN-RESERVOIR	4	512, 256, 84	16	200K	1:14:01	11/2/2024	-15	-14	-
A5	FNN-RESERVOIR	4	512, 256, 84	16	200K	-	11/2/2024	-8	-	-
A6	FNN-RESERVOIR	4	512, 256, 84	16	200K	1:27:23	11/2/2024	-12	-11	-
A7	FNN-RESERVOIR	4	512, 256, 84	16	200K	1:28:23	11/2/2024	-13	-12	-
A8	FNN-RESERVOIR	4	512, 256, 84	16	200K	1:27:01	11/2/2024	-4	-4	-
A9	FNN-RESERVOIR	4	512, 256, 84	16	200K	1:27:33	11/2/2024	-7	-6	-
A10	FNN-RESERVOIR	4	512, 256, 84	16	200K	1:09:38	11/2/2024	-11	-11	-

## B Additional Figures

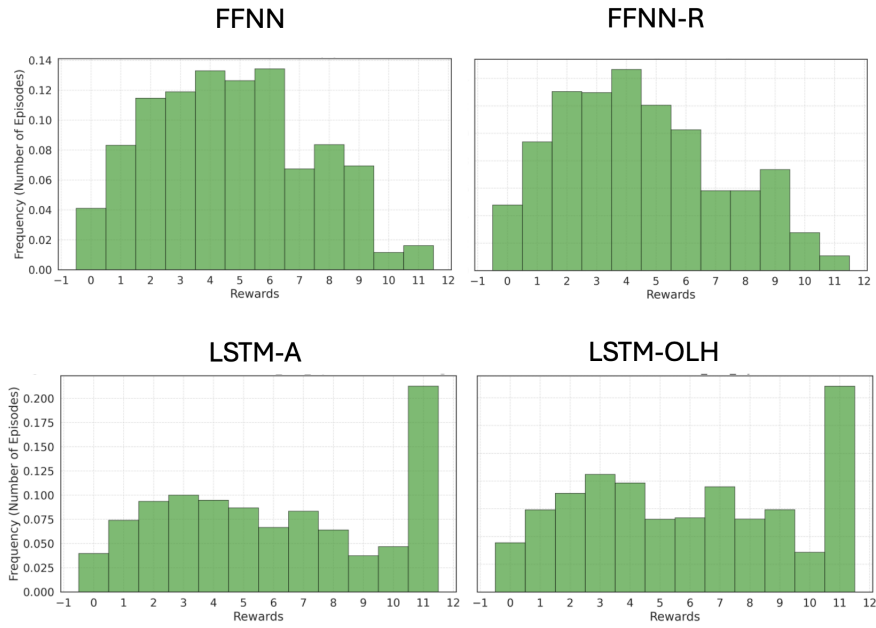


Figure B.1: Reward histograms across the four studied architectures when training for the 3d1 sequence.

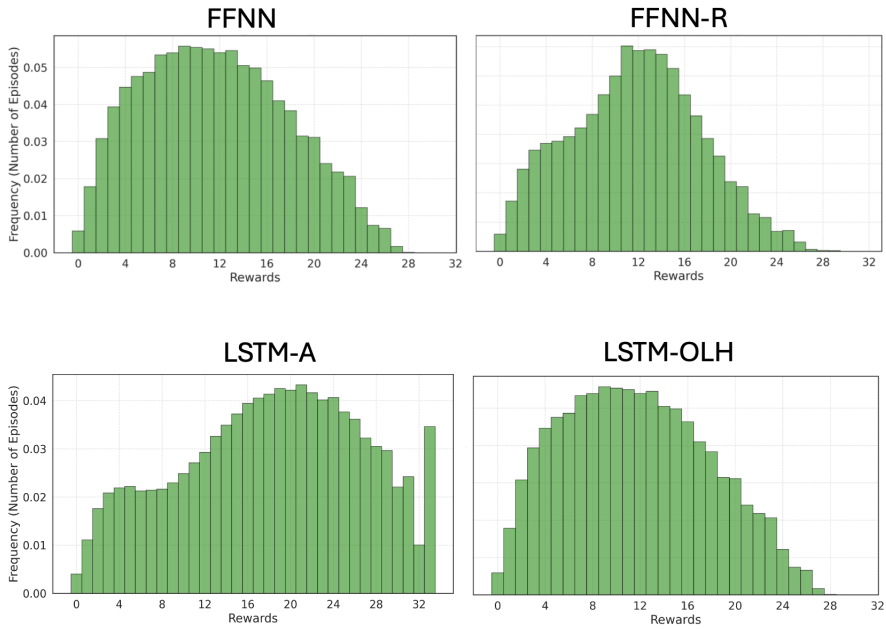


Figure B.2: Reward histograms across the four studied architectures when training for the 3d5 sequence.

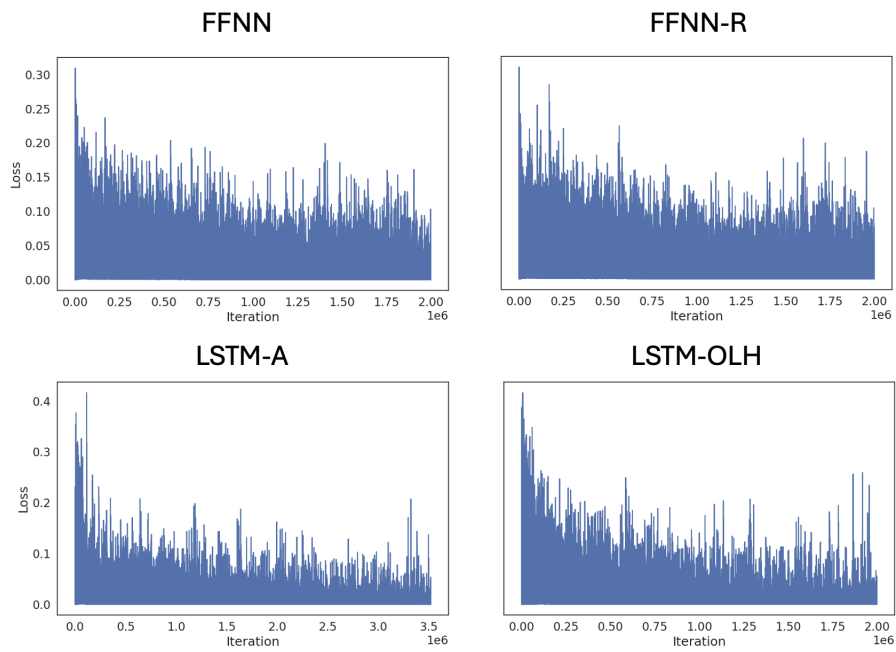


Figure B.3: Loss function across the four studied architectures when training for the 3d1 sequence.

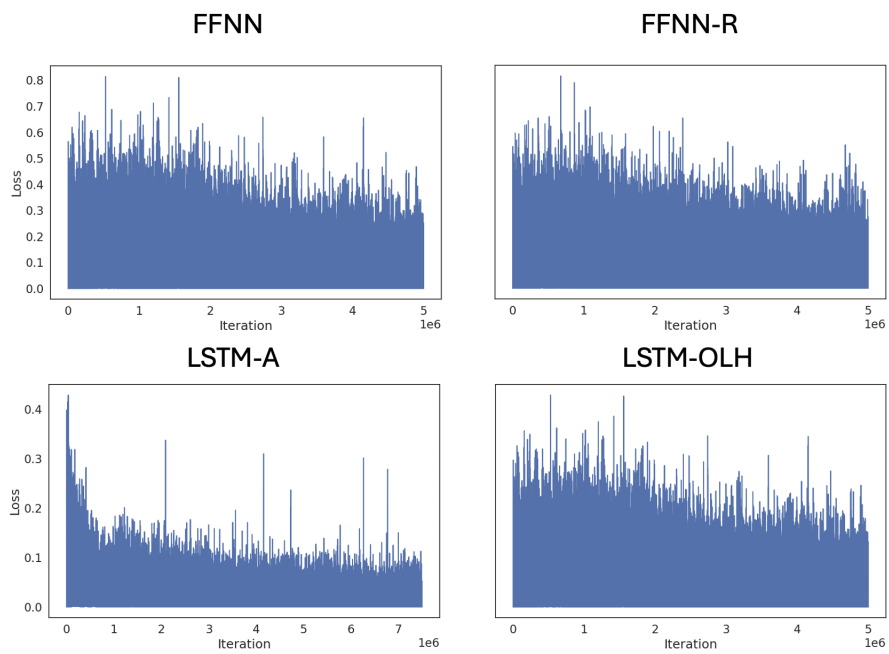


Figure B.4: Loss function across the four studied architectures when training for the 3d5 sequence.